COMSOL
CONFERENCE
2023 MUNICH

# Design of one-dimensional acoustic meta-filter with multiple resonator

M. S. Kim[1], J. Y. Lee[1]
1. CAE Solution Team, ALTSOFT Inc., Seoul, Republic of Korea.

## Abstract
New design structure for generating and tuning the multi-bands of negative modulus is presented by introducing metamaterial concept. To effectively achieve selective noise reduction and sound transmission, acoustic metamaterial consisted of arrayed multiple resonators with extended necks is proposed. Also, mathematical expression for the effective bulk modulus is developed by using a mechanical-acoustic analogy. The bandwidths and starting frequencies of multi-bands are tuned by changing only the mass ratio of the extended necks, which are converted to equivalent mass elements. Numerical investigation by using FEM simulation (Acoustics module of COMSOL Multiphysics®) is carried out to support the mathematical expression and tunability performance of multi-bands in the acoustic metamaterial. In view of the date of many passive acoustic filters and ultrasonic devices, it is expected that the proposed design structure can overcome the limitations of sound blocking in a low frequency range and precise signal transmission.

**Keywords: acoustic metamaterial, resonator, multi-bands, negative modulus**

## Introduction
Over the past few years, metamaterials which were artificially designed structures have enabled manipulation of physical phenomena beyond our knowledge [1-3]. Especially, since Fang *et al*. [4] presented an ultrasonic metamaterial consisted of arrayed Helmholtz resonators and explained its transmission characteristics by using dispersive characteristics of elastic modulus, not a few acoustic metamaterials have been proposed to exhibit unique acoustic phenomenon [5-7].

Regarding to classical issue in acoustics such as noise control [8,9], acoustic metamaterials with negative modulus [4] or negative density [7] can be advanced avenue for implementing evanescent wave phenomenon as a great alternative to attenuating sound waves [10]. In particular, due to the oscillating nature of local-resonance, dynamic effective properties with negative values generate the strong energy dissipation, resulting a stop band near the resonant frequency. Accordingly, various studies have been carried out to generate the stop band in local-resonance type acoustic metamaterials capable of achieving effective sound attenuation performance [4,7,11-13]. Several acoustic metamaterials for single-band gap have focused on generating the stop band with broad bandwidth for effective sound attenuation [7,14]. However, these acoustic metamaterials are operated at fixed frequency ranges. Thus, all geometrical parameters of the unit cell must be changed in order to shift the stop band significantly to desired frequency ranges, even if only a single stop band. In addition, generating a single-band gap is not suitable for selective noise control, which may be applied in some practical applications [15].

As one of the ways to overcome this drawback, acoustic metamaterials for multi-band gaps can be introduced that generate the new stop band by additional resonances [11-13]. Although the previous studies have proposed various attempts, however, there was no to tune the multi-band gaps, or no guideline for appropriate design of unit cell was provided. Besides, all of the aforementioned acoustic metamaterials were composed of a two-dimensional array. On the other hand, in the case of one-dimensional acoustic metamaterials, it is more suitable for applying [15] or testing [4,16] for various ideas.

In this paper, we present a new structure of acoustic metamaterial capable of generating the multi-band gaps. The proposed acoustic metamaterial consists of multiple resonators, which are designed considering the uncertainty of formula for a resonant frequency, and then develop a mathematical expression for resonant frequencies of a multiple resonator by using a mechanical-acoustic analogy. In other words, based on lumped acoustic element concept, multiple resonator can be treated as equivalent multi-degree-of-freedom vibration system, so that wave properties of acoustic metamaterial can be characterized by effective bulk modulus of its equivalent system. Also, this type of method for deriving the effective bulk modulus will facilitate the intuitional understanding of negative constitutive parameters as well as the mathematical modeling for acoustic metamaterials. The bandwidths and starting frequencies of two stop bands are tuned sensitively and precisely by changing only the mass ratio of the extended necks, which are converted to equivalent mass elements. To support the developed mathematical expression and tunability performance of stop bands in acoustic metamaterial for multi-band gaps, numerical investigations (Acoustics module of COMSOL Multiphysics®) will be shown. In view of the date of many acoustic metamaterial applications, the ability to tune the multi-band gaps may overcome the limitations of noise control devices which essentially exhibit passive responses.

## 1. Acoustic characteristics of a Helmholtz resonator

A Helmholtz resonator has been widely used as a unit cell of acoustic metamaterials for selective noise reduction of an incident acoustic wave in a frequency range of interest. In this work, a multiple resonator is used as a unit cell of acoustic metamaterials for multi-band gaps. The pass and stop bands of such resonator-type acoustic metamaterials are strongly affected by the acoustic attenuation performance of a resonator used as a unit cell. Therefore, the performance of resonator-type acoustic metamaterial for multi-bands can be derived and improved by closely investigating acoustic characteristics of single and multiple resonators.

### 1.1. Single resonator

Since Helmholtz presented it in his experiment [17], the well-known formula in Eq. (1) for a resonant frequency of a Helmholtz resonator has been used in design and theoretical analysis of a resonator for noise reduction [18]. A single resonator consists of one cavity and one neck, and their dimensions satisfying Eq. (1) are tuned to adjust the resonant frequency ($f_r$) to a target frequency ($f_t$) for noise reduction in a square cross-sectional duct with a side of $h_d$ in Fig. 1.

$$f_r = \frac{c}{2\pi}\sqrt{\frac{S_n}{V_c L_n'}} \tag{1a}$$

$$L_n' = L_n + \delta,\ \delta = 1.7\sqrt{\frac{S_n}{\pi}} \tag{1b}$$

where $S_n$ and $L_n$ represent the cross-sectional area and length of a neck, respectively, and $L_n'$ and $V_c$ are an effective length of a neck including an end correction ($\delta$) and the cavity volume, respectively. The speed of sound in acoustic media (air) of a duct is denoted by $c$. Since the formula in Eq. (1) allows the resonator designers to freely select the shape of a cavity and the cross section of a neck, it is assumed that a resonator in this work consists of a rectangular parallelepiped cavity and a rectangular parallelepiped neck, as shown in Fig. 1.

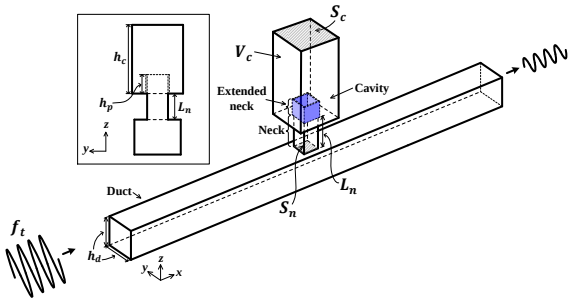


*Figure 1. Single Helmholtz resonator with an extended neck installed at a square cross-sectional duct.*

The formula in Eq. (1) is derived by using the mechanical-acoustic analogy under the assumptions of $L_n \ll \lambda$, $\sqrt{S_n} \ll \lambda$ and $\sqrt[3]{V_c} \ll \lambda$, where $\lambda$ is a wavelength [19]. The lumped acoustic elements can be converted to equivalent vibration elements; a cavity and a neck are replaced with a spring and a mass, respectively. The equivalent mass ($m_{\mathrm{eq}}$) and spring constant ($k_{\mathrm{eq}}$) are expressed as in Eq. (2).

$$m_{\mathrm{eq}} = \rho S_n L_n' \tag{2a}$$

$$k_{\mathrm{eq}} = \rho c^2 S_n^2 / V_c \tag{2b}$$

where $\rho$ is the fluid density in a resonator. It is worth mentioning that various combinations of $S_n$, $L_n$ and $V_c$ exist for a target frequency because Eq. (1) has no special constraints on three unknown parameters ($S_n$, $L_n$ and $V_c$) satisfying the design condition of $f_t = f_r$. For duct noise reduction, however, a combination of $S_n$, $L_n$ and $V_c$ must be selected so that the peak frequency in a transmission loss (TL) curve of a resonator should be equal to $f_t$.

Considering $f_r = (1/2\pi)\sqrt{k_{\mathrm{eq}}/m_{\mathrm{eq}}}$, the neck's length and the cavity volume should be increased or the neck's cross-sectional area should be decreased for a lower resonant frequency, and vice-versa. An extended neck as shown in Fig. 1 can be considered as an alternative method to increase the equivalent mass of a neck without increasing the value of $L_n$. In this case, Eq. (1b) is replaced by $L_n' = L_n + h_p + \delta$, where $h_p$ is the extended length of the neck. This means that the extended neck enables us to increase an equivalent mass of a resonator without increasing the outer length ($L_n$) of a neck for a lower resonant frequency.

### 1.2. Multiple resonator

As shown in Fig. 2(a), the multiple resonator consisting of more than two resonators can be converted to an equivalent multi-degree-of-freedom vibration system under the same assumptions as those for a single resonator.

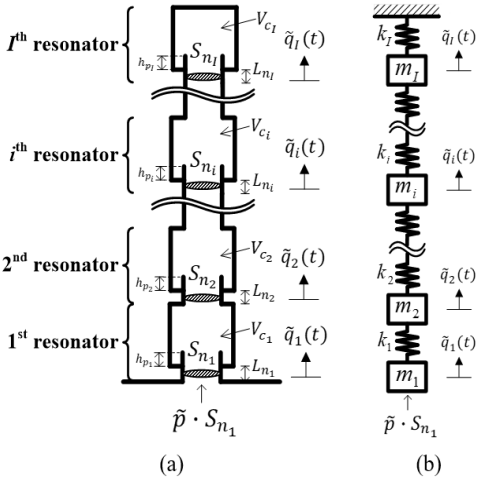


*Figure 2. Schematics of (a) multiple resonator and (b) equivalent multi-degree-of-freedom vibration system.*

Each resonator has its extended neck. Assuming the harmonic motion of each equivalent mass and acoustic pressure ($\tilde{q}_i(t) = q_i e^{j\omega t}$ and $\tilde{p} = p e^{j\omega t}$ with $j = \sqrt{-1}$), the governing equation in Eq. (3)

with Eq. (4) is obtained for the equivalent vibration system in Fig. 2(b). When each resonator is installed at a duct as a single resonator as shown in Fig. 1, its resonant frequency is denoted by $f_i = (1/2\pi)\sqrt{k_i/m_i}$, where $k_i$ and $m_i$ are equivalent stiffness and mass, respectively. They are functions of the dimensions of each resonator as expressed in Eq. (5). The resonant frequencies ($f_i^*$) of a multiple resonator are calculated from Eq. (6a), and the displacement of the 1st equivalent mass ($m_1$) is expressed as in Eq. (6b). The detailed procedure is explained in Appendix.

$$[\mathbf{K}]\mathbf{Q} = \mathbf{F} \tag{3a}$$

$$\mathbf{Q} = [\tilde{q_1}\ \tilde{q_2}\cdots\tilde{q_i}\cdots\tilde{q_I}]^T,\ \mathbf{F} = [\tilde{p}S_{n_1}\ 0\cdots 0\cdots 0]^T \tag{3b}$$

$$[\mathbf{K}] = \begin{bmatrix} K_{1,1} & K_{1,2} & 0 & 0 & 0 & \cdots & \cdots & 0 \\ K_{2,1} & K_{2,2} & K_{2,3} & 0 & \vdots & \vdots & \vdots & 0 \\ 0 & K_{3,2} & \ddots & \ddots & \ddots & \ddots & \vdots & \vdots \\ \vdots & 0 & \ddots & \ddots & K_{i-1,i} & \ddots & 0 & \vdots \\ \vdots & \vdots & \ddots & K_{i,i-1} & K_{i,i} & K_{i,i+1} & \ddots & \vdots \\ \vdots & \vdots & \vdots & 0 & K_{i+1,i} & \ddots & \ddots & 0 \\ \vdots & \vdots & \vdots & \vdots & \ddots & \ddots & \ddots & K_{I-1,I} \\ 0 & 0 & 0 & 0 & \cdots & 0 & K_{I,I-1} & K_{I,I} \end{bmatrix} \tag{3c}$$

$$K_{1,1} = k_1 - m_1\omega^2,\ \omega = 2\pi f \tag{4a}$$

$$K_{i,i} = m_i\omega^2 - k_{i-1} - k_i,\ (i = 2,3,\cdots,I) \tag{4b}$$

$$K_{1,2} = -k_1,\ K_{2,1} = k_1 \tag{4c}$$

$$K_{i,i+1} = K_{i+1,i} = k_i,\ (i = 2,3,\cdots,I-1) \tag{4d}$$

$$m_i = \rho S_{n_i} L'_{n_i},\ k_i = \rho c^2 \frac{S_{n_i}^2}{V_{c_i}} \tag{5a}$$

$$L'_{n_i} = L_{n_i} + h_{p_i} + \delta_i,\ \delta_i = 1.7\sqrt{\frac{S_{n_i}}{\pi}} \tag{5b}$$

$$\det[\mathbf{K}] = 0 \tag{6a}$$

$$\tilde{q}_1 = \frac{C_{1,1}\tilde{p}\cdot S_{n_1}}{\det[\mathbf{K}]} = \frac{M_{1,1}\tilde{p}\cdot S_{n_1}}{\sum_{j=1}^{I}(-1)^{j+k}K_{j,k}M_{j,k}} \tag{6b}$$

The resonant frequencies ($f_1^*$ and $f_2^*$) of a double resonator are obtained from the characteristic equation as expressed in Eq. (7a). The displacement of the 1st equivalent mass of a double resonator is expressed as in Eq. (7b). The coefficients in the characteristic equation include the mass ratio of necks as well as resonant frequencies of single resonators.

$$\omega^4 - (\omega_1^2/\theta_1 + \omega_1^2 + \omega_2^2)\omega^2 + \omega_1^2\omega_2^2 = 0,\quad \theta_1 = m_2/m_1 \tag{7a}$$

$$\tilde{q}_1 = \frac{\tilde{p}S_{n_1}K_{2,2}}{K_{1,1}K_{2,2} - K_{1,2}K_{2,1}} \tag{7b}$$

Fig. 3 compares the TL curves of the double resonators of different mass ratios for four cases; Case 1-1 to 1-4. All single resonators are tuned for the same resonant frequency ($f_r = 300$ Hz), and the resonant frequencies ($f_1^*$ and $f_2^*$) and the mass ratios ($m_2/m_1$) of all double resonators are summarized in Table 1 (Specific values of geometric parameters of the resonators are summarized in Table 2).

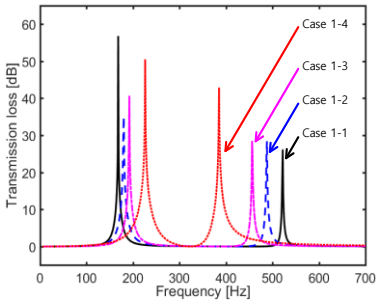


*Figure 3. Numerically calculated transmission loss of double resonators depending on mass ratio.*

| Case | Double resonator: 1st resonator | Double resonator: 2nd resonator | $f_1^*$ [Hz] | $f_2^*$ [Hz] | $m_2/m_1$ |
|---|---|---|---|---|---|
| 1-1 | Resonator F | Resonator A | 168 | 522 | 0.75 |
| 1-2 | Resonator A | Resonator A | 180 | 488 | 1.00 |
| 1-3 | Resonator A | Resonator F | 192 | 456 | 1.34 |
| 1-4 | Resonator D | Resonator E | 226 | 385 | 4.98 |

***Table 1**: Resonant frequencies and mass ratios for various combinations of Case 1.*

| Symbol | R-A | R-B | R-C | R-D | R-E | R-F |
|---|---|---|---|---|---|---|
| $L_n$ [mm] | 34 | 13 | 55 | 5 | 75 | 34 |
| $S_n$ [mm²] | 13.14 × 13.14 | | | | | |
| $h_c$ [mm] | 106.09 | 146.8 | 75.36 | 167.12 | 37.28 | 79 |
| $S_c$ [mm²] | 34 × 34 | 39 × 39 | 33.5 × 33.5 | 35 × 55.5 | 35 × 50 | 34 × 34 |
| $h_p$ [mm] | 0 | 0 | 0 | 0 | 0 | 21.08 |

***Table 2**: Specific values of geometric parameters of Resonator A to F (R-A, R-B, R-C, R-D, R-E and R-F).*

As the mass ratio increases, the first peak frequency ($f_1^*$) of the double resonator increases and its second peak frequency ($f_2^*$) decreases. It implies that the mass ratio can change the difference between two resonant frequencies of a double resonator. The fact could be used for tuning the multi-bands of a multiple resonator-type acoustic metamaterial as well as a double resonator-type acoustic metamaterial.

## 2. Effective bulk modulus for acoustic metamaterial with a multiple resonator

Fig. 4(a) shows a unit cell used to develop the effective bulk modulus of the acoustic metamaterial. In the unit cell model, a control volume ($V$) in a duct is surrounded by imaginary surfaces, which are represented by broken lines, in a stationary state. The control volume of a duct changing due to pressure difference between both sides of the control volume is denoted by $V'$, which is surrounded by dashed-dotted lines. A net volume change ($\Delta V_{\text{net}}$) through the imaginary surfaces surrounding the control volume consists of volume change ($\Delta V$) in a duct and volume change ($\Delta V_r$) in the 1st resonator's neck, as expressed in Eq. (8).

$$\Delta V_{\text{net}} = \Delta V + \Delta V_r \tag{8}$$

Fig. 4(b) shows an equivalent duct, where the bulk modulus ($B$) is replaced with an effective bulk modulus ($B_{\text{eff}}$).

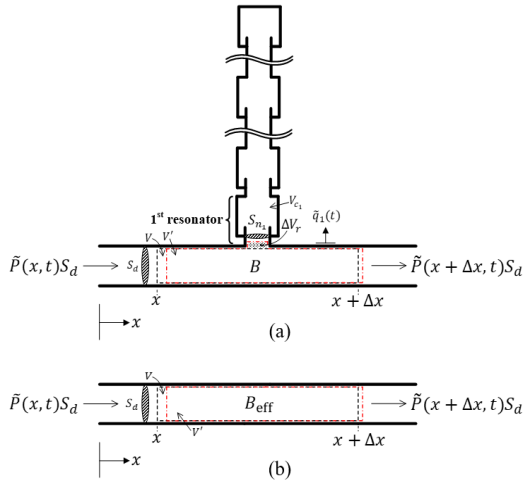


*Figure 4. Schematics of (a) unit cell and (b) equivalent system for the unit cell.*

A bulk modulus in a duct connected with a multiple resonator in Fig. 4(a) and the effective bulk modulus in Fig. 4(b) are defined as in Eqs. (9a) and (9b), respectively.

$$B = -V\frac{\Delta\tilde{P}}{\Delta V_{\text{net}}} \quad (9a)$$

$$B_{\text{eff}} = -V\frac{\Delta\tilde{P}}{\Delta V} \quad (9b)$$

From Eqs. (8), (9a) and (9b), the effective bulk modulus is expressed as a function of the ratio between $\Delta V_r$ and $\Delta V$ as in Eq. (10a). Using $\Delta V_r = S_{n_1}\widetilde{q_1}$, Eq. (10a) is converted to Eq. (10b).

$$B_{\text{eff}} = B(1 + \Delta V_r/\Delta V) \quad (10a)$$

$$B_{\text{eff}} = B(1 + \widetilde{q_1}S_{n_1}/\Delta V) \quad (10b)$$

Recalling that the acoustic pressure is approximately equal to the pressure difference ($\tilde{p} \cong \Delta\tilde{P}$), the effective bulk modulus of an acoustic metamaterial with a multiple resonator is expressed as in Eq. (11a), and it is simplified to Eqs. (11b) and (11c) when double and triple resonator are used as a unit cell, respectively.

$$B_{\text{eff}}^{-1}(\omega) = B^{-1}\left[1 + \frac{V_{c_1}}{V}\frac{M_{1,1}k_1}{\sum_{j=1}^{I}(-1)^{j+k}K_{j,k}M_{j,k}}\right],$$

$$(k = 1, 2, \cdots, I),\ I \geq 2 \quad (11a)$$

$$B_{\text{eff}}^{-1}(\omega) = B^{-1}\left[1 + \frac{V_{c_1}}{V}\frac{k_1}{K_{1,1}-K_{1,2}K_{2,1}/K_{2,2}}\right] \quad (11b)$$

$$B_{\text{eff}}^{-1}(\omega) = B^{-1}\left[1 + \frac{V_{c_1}}{V}\frac{K_{2,2}K_{3,3}-k_2^2}{K_{1,1}K_{2,2}K_{3,3}/k_1 - K_{1,1}k_2^2/k_1 + k_1K_{3,3}}\right] \quad (11c)$$

In Eq. (11b), if $m_2$ increases infinitely, the effective bulk modulus for a double resonator is simplified to Eq. (12), which is the same one as presented for a single resonator in Ref. [4]; the expression was derived by using an acoustic-electrical analogy for a single resonator.

$$B_{\text{eff}}^{-1}(\omega) = B^{-1}\left[1 - \frac{F_1\omega_1^2}{\omega^2-\omega_1^2}\right],\ \omega_1 = \sqrt{\frac{k_1}{m_1}},$$

$$F_1 = \frac{V_{c_1}}{V} \quad (12)$$

Fig. 5(a) compares the effective bulk modulus curve, which is plotted on a log scale, and the transmission coefficient curve, which is plotted on a linear scale, of an acoustic metamaterial with a double resonator, which consists of Resonator B (the 1st resonator) and Resonator C (the 2nd resonator). The resonant frequencies ($f_1^*$ and $f_2^*$) of the double resonator are 212 and 420 Hz. The acoustic metamaterial consists of 24 unit cells, and the subwavelength separation between the arrayed double resonators is much less than the wavelength in interest ($\Delta x = 0.04$ m $\sim \lambda/30$). In the frequency range of negative modulus ($B_{\text{eff}} < 0$) which is represented by light orange colored rectangles, the transmission coefficient ($|t|$) is extremely low.

Fig. 5(b) compares the propagations of incident acoustic pressure in a duct depending on its frequencies (250, 365, 500 Hz). At the two frequencies (250 and 500 Hz) in the stop bands, the incident acoustic wave with a higher magnitude at the left end was decayed extremely after passing the third unit cell. In contrast, an incident acoustic wave at 365 Hz in the pass band is freely transmitted to the other end of a duct.

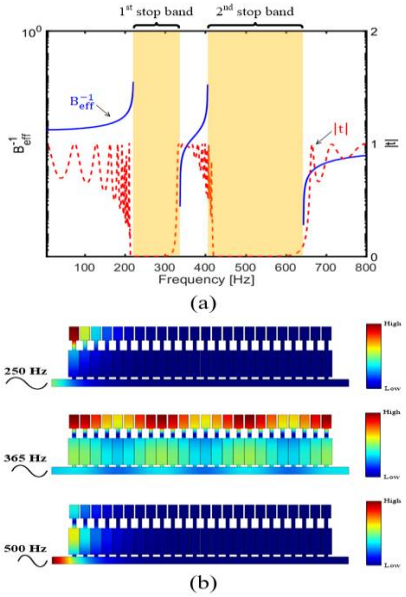


*Figure 5. (a) Effective bulk modulus and numerically calculated transmission coefficient and (b) propagations of incident acoustic waves depending on frequency.*

## 3. Effects of necks' mass ratio on stop and pass bands

### 3.1. Double resonator consisting of two resonators of the same resonant frequencies

As seen in Fig. 5(a), the starting frequencies of the stop bands are approximately equal to the resonant frequencies ($f_1^*$ and $f_2^*$) of a double resonator, which change due to mass ratio of two necks, as observed in subsection 1.2. In this section, we investigate the effect of necks' mass ratio on the

stop bands of the acoustic metamaterial when two resonators of a double resonator have the same resonant frequencies ($f_1$ and $f_2$) and different dimensions. Four cases are considered depending on the mass ratio as summarized in Table 1. Fig. 6(a) compares the transmission coefficient curves of four cases. As the mass ratio increases, the 1st stop band becomes narrower but the 2nd stop band becomes wider. This phenomenon results from the change of the resonant frequencies ($f_1^*$ and $f_2^*$) of each double resonator, which approximately coincides with the starting frequencies of stop bands, as investigated in the previous section. Also, this change makes the pass band between two stop bands decrease or increase. The changing trend in stop bands approximately coincides with the change in frequency band of negative values of the effective bulk modulus curve in Fig. 6(b).

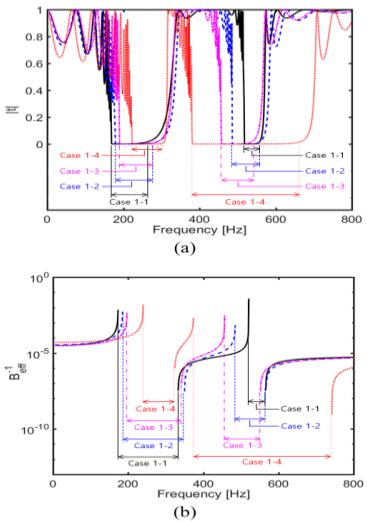


*Figure 6. (a) Numerically calculated transmission coefficients and (b) effective bulk modulus of acoustic metamaterials with double resonators in Case 1.*

Investigation on the combination of two resonators in each case gives an interesting insight. First, Cases 1-1 and 1-3 used the same pairs of resonators but different connecting order; Resonator F in the 1st resonator and Resonator A in the 2nd resonator in Case 1-1, and Resonator A in the 1st resonator and Resonator F in the 2nd resonator in Case 1-3. While the 1st stop band in Case 1-1 is wider than that in Case 1-3, the 2nd stop band in Case 1-1 is narrower than that in Case 1-3. Second, since Resonator F included an extended neck, the equivalent mass of the resonator could be much increased without an increase in its outer dimensions.

### 3.2. Double resonator consisting of two resonators of the different resonant frequencies

This section investigates the acoustic transmission characteristics of a double resonator consists of two single resonators, whose resonant frequencies do not coincide with each other. In the first case study (Case 2), the resonant frequencies ($f_1$ and $f_2$) of the 1st and 2nd resonators are tuned to 300 and 600 Hz, respectively. In the second case study (Case 3), the resonant frequencies are tuned to 600 and 300 Hz, respectively. Dimensions of additionally used resonators and the combination of single resonators in each double resonator are summarized in Tables 3 and 4.

| Symbol | R-G | R-H | R-I | R-J | R-K |
|---|---|---|---|---|---|
| $L_n$ [mm] | 10 | 30 | 42.5 | 7.5 | 5 |
| $S_n$ [mm²] | | | | | |
| $h_c$ [mm] | 80.37 | 53.68 | 23.11 | 85.72 | 90.53 |
| $S_c$ [mm²] | 28.05 × 28.05 | 25 × 25 | 33.5 × 33.5 | 28.8 × 28.8 | 29.95 × 29.95 |

***Table 3**: Specific values of geometric parameters of Resonator G to L (R-G, R-H, R-I, R-J and R-K).*

| Case | Double resonator | | $f_1^*$ [Hz] | $f_2^*$ [Hz] | $m_2/m_1$ |
|---|---|---|---|---|---|
| | 1st resonator | 2nd resonator | | | |
| 2-1 | Resonator A | Resonator G | 231 | 718 | 0.49 |
| 2-2 | Resonator B | Resonator H | 269 | 637 | 1.66 |
| 2-3 | Resonator D | Resonator I | 277 | 621 | 3.13 |
| 3-1 | Resonator G | Resonator A | 224 | 770 | 2.06 |
| 3-2 | Resonator J | Resonator C | 241 | 713 | 3.36 |
| 3-3 | Resonator K | Resonator E | 251 | 680 | 4.98 |

***Table 4**: Resonant frequencies and mass ratios for various combinations of Cases 2 and 3.*

Fig. 7 compares the transmission coefficient curves of Cases 2 and 3. In all cases, the transmission coefficient curves have two stop bands, which were determined by using the criterion of $|t| \leq 10^{-2}$.

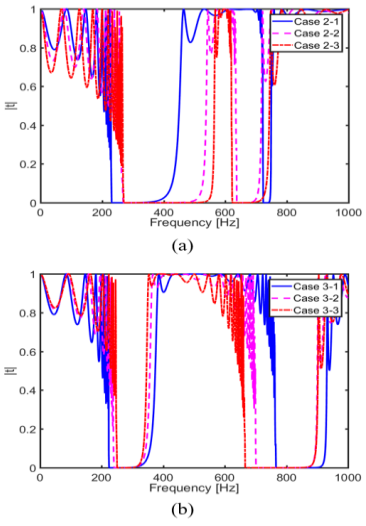


*Figure 7. Transmission coefficients of acoustic metamaterials with double resonators in (a) Case 2 and (b) Case 3.*

While the starting frequency of the 1st stop band increases with the mass ratio, that of the 2nd stop band decreases with the increasing mass ratio. This

result coincides with the phenomenon observed in the previous subsection, and it is due to the change of the resonant frequencies ($f_1^*$ and $f_2^*$) of the double resonator changing with the mass ratio as summarized in Table 4. The bandwidths of the 1st and 2nd stop bands are strongly correlated with single resonators tuned to 300 and 600 Hz, respectively. Therefore, the bandwidths of two stop bands are different depending on the order of two resonators, i.e., resonant frequency ratios ($f_2/f_1$) of the two single resonators; while the 1st stop band is wider than the 2nd stop band in Case 2, the 2nd stop band is wider than the 1st stop band in Case 3.

### 3.3 Normalized bandwidth of a double resonator

The frequency range (bandwidth) of each stop band of a double resonator-type acoustic metamaterial can be obtained analytically from the condition of $B_{\text{eff}}(\omega) < 0$ and is expressed in Eq. (13) with its lower and upper limit frequencies ($f_{l_i}^*$ and $f_{u_i}^*$). The lower limit frequencies of each stop bands are resonant frequencies of a double resonator, which are calculated from Eq. (7a), and the lower and upper limit frequencies are expressed by using the resonant frequencies ($f_1$ and $f_2$) of a double resonator and the mass ratio ($m_2/m_1$) of its necks as shown in Eqs. (13b) and (13c).

$$f_{l_i}^* < f < f_{u_i}^*, (i = 1, 2) \quad (13a)$$

$$\left.\begin{matrix}\left(\frac{f_{l_1}^*}{f_1}\right)^2 \\ \left(\frac{f_{l_2}^*}{f_1}\right)^2\end{matrix}\right\} = \frac{1+\theta_1\left\{1+\left(\frac{f_2}{f_1}\right)^2\right\} \pm \left[\left[1+\theta_1\left\{1+\left(\frac{f_2}{f_1}\right)^2\right\}\right]^2 - 4\theta_1^2\left(\frac{f_2}{f_1}\right)^2\right]^{\frac{1}{2}}}{2\theta_1},$$

$$\theta_1 = m_2/m_1 \quad (13b)$$

$$\left.\begin{matrix}\left(\frac{f_{u_1}^*}{f_1}\right)^2 \\ \left(\frac{f_{u_2}^*}{f_1}\right)^2\end{matrix}\right\} = \frac{\left[\begin{matrix}1+(1+F_1)\theta_1+\theta_1+\left(\frac{f_2}{f_1}\right)^2 \\ \pm\left[\left\{1+(1+F_1)\theta_1+\theta_1\left(\frac{f_2}{f_1}\right)^2\right\}^2 - 4\theta_1\left[(1+F_1)\left\{1+\left(\frac{f_2}{f_1}\right)^2\theta_1\right\}-1\right]\right]^{\frac{1}{2}}\end{matrix}\right]}{2\theta_1},$$

$$\theta_1 = m_2/m_1 \quad (13c)$$

where $F_1$ is the ratio of the cavity volume (1st resonator) and the control volume, i.e., $F_1 = V_{c_1}/V$.

Fig. 8(a) shows the normalized resonant frequencies of the double resonator depending on the mass ratio for various resonant frequency ratios ($f_2/f_1$) of the two single resonators. The normalized resonant frequencies are calculated by dividing the resonant frequencies ($f_1^*$ and $f_2^*$) of the double resonator by the lowest one ($f_1$) among the resonant frequencies of two single resonators. The lower limit frequencies of the two stop bands increase with the $f_2/f_1$. The difference between the starting frequencies (lower limit frequencies) decreases with the increasing mass ratio and becomes a minimum value for $f_2/f_1 = 1$.

Fig. 8(b) shows the normalized bandwidths of two stop bands depending on the mass ratio for various resonant frequency ratios ($f_2/f_1$) of the two single resonators. The normalized bandwidths are calculated by dividing the bandwidth ($f_{u_i}^* - f_{l_i}^*$) of each stop band by lowest one ($f_1$) among the resonant frequencies of two single resonators. For each case of $f_2/f_1$, all normalized bandwidths of two stop bands generally increase with the mass ratio until the crossing point where the normalized bandwidths of two stop bands become equal to each other. However, after the crossing point, the change of each normalized bandwidth of two stop bands shows a truly opposite trend depending on the mass ratio. Also, the mass ratio corresponding to the crossing point increases with the resonant frequency ratios ($f_2/f_1$) of two resonators.

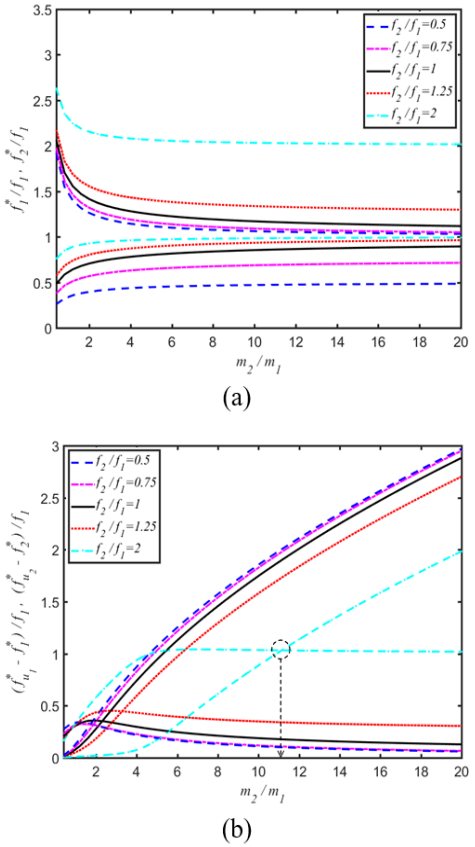


*Figure 8. (a) Normalized resonant frequencies of the double resonator as a function of the mass ratio for various resonant frequency ratios ($f_2/f_1$) and (b) normalized bandwidths of two stop bands as a function of the mass ratio for various frequency ratios.*

## Conclusions

New acoustic metamaterial with multi-bands of negative modulus was presented. The proposed acoustic metamaterial consists of a duct and arrayed multiple resonators with extended necks, and all resonators in each multiple resonator have the same or different resonant frequencies each other. The mathematical expression for the effective bulk modulus was developed first for a double resonator with extended necks, which is simplified into equivalent two-degree-of-freedom vibration system, and was extended for a multiple resonator. The

bandwidths and starting frequencies (resonant frequencies) of two stop bands can be tuned by varying only the mass ratio of extended necks, which are converted to equivalent mass elements. From the mathematical expression for the negative modulus, analytical results that can serve as an appropriate guideline for the design of acoustic metamaterial with multi-bands was derived. The proposed acoustic metamaterial, namely, acoustic meta-filter, is expected to be applicable to selective noise reduction in a low frequency range and signal transmission in ultrasonic devices.

## References


[1] S. Zhang, et al., "Negative refractive index in chiral metamaterials", *Physical review letters*, 102(2): 023901, 2009.

[2] S. H. Lee, et al., "Reversed Doppler effect in double negative metamaterials", *Physical Review B*, 81(24): 241102, 2010.

[3] X. Chen, et al., "Three-dimensional broadband and high-directivity lens antenna made of metamaterials", *Journal of Applied Physics*, 110(4), 2011.

[4] N. Fang, et al., "Ultrasonic metamaterials with negative modulus", *Nature materials*, 5(6): 452-456, 2006.

[5] H. Chen and C. T. Chan, "Acoustic cloaking in three dimensions using acoustic metamaterials", *Applied physics letters*, 91(18), 2007.

[6] S. Guenneau, et al., "Acoustic metamaterials for sound focusing and confinement", *New Journal of physics*, 9(11): 399, 2007.

[7] Z. Yang, et al., "Acoustic metamaterial panels for sound attenuation in the 50–1000 Hz regime", *Applied Physics Letters*, 96(4), 2010.

[8] G. F. Butler, "A note on improving the attenuation given by a noise barrier", *Journal of Sound and Vibration*, 32(3): 367-369, 1974.

[9] J. M. De Bedout, et al., "Adaptive-passive noise control with self-tuning Helmholtz resonators", *Journal of Sound and Vibration*, 202(1): 109-123, 1997.

[10] M. R. Haberman and M. D. Guild, "Acoustic metamaterials", *Physics Today*, 69(6): 42-48, 2016.

[11] C. L. Ding and X. P. Zhao, "Multi-band and broadband acoustic metamaterial with resonant structures". *Journal of Physics D: Applied Physics*, 44(21): 215402, 2011.

[12] V. Romero-García, et al., "Multi-resonant scatterers in sonic crystals: Locally multi-resonant acoustic metamaterial", *Journal of Sound and Vibration*, 332(1): 184-198, 2013.

[13] S. Cho, et al., "Tunable two-dimensional acoustic meta-structure composed of funnel-shaped unit cells with multi-band negative acoustic property", *Journal of Applied Physics*, 118(16), 2015.

[14] J. W. Jung, et al., "Acoustic metamaterial panel for both fluid passage and broadband soundproofing in the audible frequency range", *Applied Physics Letters*, 112(4), 2018.

[15] A. J. LeRoy and J. W. Segura., "Percutaneous ultrasonic lithotripsy", *Urologic radiology*, 6: 88-94, 1984.

[16] G. Wang, et al., "Quasi-one-dimensional periodic structure with locally resonant band gap", *Journal of Applied Mechanics*, 73: 167-170, 2006.

[17] H. L. Helmholtz, "On the sensation of tones", New York (Reproduced in 1954 by Dover Publication Inc.), 1877.

[18] U. Ingard. "On the theory and design of acoustic resonators", *The Journal of the acoustical society of America*, 25(6): 1037-1061, 1953.

[19] L. E. Kinsler, et al., "Fundamentals of acoustics", John wiley & sons, 2000.

[20] E. Krevszig. "Advanced Engineering Mathematics", John Wiley & Sons Inc., 2004.


## Appendix

As shown in Eq. (3c), the stiffness matrix of multi-degree-of-freedom vibration system in Fig. 2(b) is expressed as

$$[\mathbf{K}]=\begin{bmatrix} K_{1,1} & K_{1,2} & 0 & 0 & 0 & \cdots & \cdots & 0 \\ K_{2,1} & K_{2,2} & K_{2,3} & 0 & \vdots & \vdots & \vdots & 0 \\ 0 & K_{3,2} & \ddots & \ddots & \ddots & \ddots & \vdots & \vdots \\ \vdots & 0 & \ddots & \ddots & K_{i-1,i} & \ddots & 0 & \vdots \\ \vdots & \vdots & \ddots & K_{i,i-1} & K_{i,i} & K_{i,i+1} & \ddots & \vdots \\ \vdots & \vdots & \vdots & 0 & K_{i+1,i} & \ddots & \ddots & 0 \\ \vdots & \vdots & \vdots & \vdots & \ddots & \ddots & \ddots & K_{I-1,I} \\ 0 & 0 & 0 & 0 & \cdots & 0 & K_{I,I-1} & K_{I,I} \end{bmatrix}. \quad \text{(A1)}$$

Then, a determinant of an $I \times I$ matrix $[\mathbf{K}] = [K_{j,k}]$ for $I \geq 2$ is expressed as in Eq. (A2) [20]:

$$\det[\mathbf{K}] = K_{j,1}C_{j,1} + K_{j,2}C_{j,2} + \cdots + K_{j,I}C_{j,I}, \quad (j = 1,2,\cdots,I) \text{ (A2)}$$

$$C_{j,k} = (-1)^{j+k}M_{j,k} \quad \text{(A3)}$$

where $M_{j,k}$ is a determinant of order $I-1$, namely, the determinant of the submatrix of $[\mathbf{K}]$ obtained from $[\mathbf{K}]$ by omitting the row and column of the entry $K_{j,k}$, that is, the $j^{th}$ row and the $k^{th}$ column. In this way, $\det[\mathbf{K}]$ is defined in terms of $I$ determinants of order $I-1$, each of which is, in turn, defined in terms of $I-1$ determinants of order $I-2$, and so on – until we finally arrive at second-order determinants. Note that, $M_{j,k}$ is called the minor of $K_{j,k}$ in $\det[\mathbf{K}]$, and $C_{j,k}$ the cofactor of $K_{j,k}$ in $\det[\mathbf{K}]$. Eq. (A2) may also be written in terms of minors.

$$\det[\mathbf{K}] = \sum_{k=1}^{I}(-1)^{j+k}K_{j,k}M_{j,k}, (j = 1,2,\cdots,I) \text{ (A4)}$$

To determine the inverse $[\mathbf{K}]^{-1}$ of a nonsingular $I \times I$ matrix $[\mathbf{K}]$, we can use a variant of the Gauss elimination, called the Gauss-Jordan elimination [20].

$$[\mathbf{K}]^{-1} = \frac{1}{\det[\mathbf{K}]}[C_{j,k}]^T = \frac{1}{\det[\mathbf{K}]}\begin{bmatrix} C_{1,1} & C_{2,1} & \cdots & C_{I,1} \\ C_{1,2} & C_{2,2} & \cdots & C_{I,2} \\ \cdot & \cdot & \cdots & \cdot \\ C_{1,I} & C_{2,I} & \cdots & C_{I,I} \end{bmatrix} \text{ (A5)}$$

Now, substituting Eq. (A5) in the governing equation (A6), displacement matrix is derived as in Eq. (A8) where the $\mathbf{F} = [\tilde{p} \cdot S_{n_1} 0 \cdots 0 \cdots 0]^T$.

$$[\mathbf{K}]\mathbf{Q} = \mathbf{F} \quad \text{(A6)}$$

$$\mathbf{Q} = [\mathbf{K}]^{-1}\mathbf{F} \quad \text{(A7a)}$$

$$[\tilde{q}_1\ \tilde{q}_2\ \cdots\ \tilde{q}_i\ \cdots \tilde{q}_I\ ]^T = \frac{1}{\det[\mathbf{K}]}\begin{bmatrix} C_{1,1} & C_{2,1} & \cdots & C_{I,1} \\ C_{1,2} & C_{2,2} & \cdots & C_{I,2} \\ \cdot & \cdot & \cdots & \cdot \\ C_{1,I} & C_{2,I} & \cdots & C_{I,I} \end{bmatrix}[\tilde{p} \cdot S_{n_1} 0 \cdots 0 \cdots 0]^T \text{ (A7b)}$$

Finally, displacement of the 1st equivalent mass ($m_1$) can be achieved as

$$\tilde{q}_1 = \frac{C_{1,1}\tilde{p}\cdot S_{n_1}}{\det[\mathbf{K}]} = \frac{M_{1,1}\tilde{p}\cdot S_{n_1}}{\sum_{j=1}^{I}(-1)^{j+k}K_{j,k}M_{j,k}}. \quad \text{(A8)}$$